JOURNAL OF PROPULSION AND POWER
Vol. 23, No. 1, January–February 2007

Variation of Vortex Structure in a Compressor Cascade at Different Incidences

Hualiang Zhang,* Songtao Wang,† and Zhongqi Wang‡
Harbin Institute of Technology, 150001 Heilongjiang, People's Republic of China

DOI: 10.2514/1.17245

Based on experimental results, a numerical study was performed to analyze the flow pattern and the vortex structure in a compressor cascade at different incidences using the topological principles as well as the critical principles of the three-dimensional separation. The results show that the topology of the critical points on the suction surface varies with the incidence and that the separation type changes to closed separation from open separation. In addition, the passage vortex is a classical open separation. The horseshoe vortex and the corner vortex belong to closed separation. Finally, the authors propose a new model of the vortex structure in a compressor cascade.

Nomenclature

CV	=	corner vortex
HP	=	pressure side leg of the horseshoe vortex
HS	=	suction side leg of the horseshoe vortex
$\bar{h}$	=	relative height of the blade
h_1, h_2	=	distance from the wall
k	=	specific heat ratio of air
N	=	nodal point
P	=	static pressure
P^*	=	total pressure
PS	=	pressure side of the cascade
PV	=	passage vortex
S	=	saddle point
SS	=	suction side of the cascade
SV	=	tailing shedding vortex
u, v, w	=	velocity components in the three directions
x, y, z	=	Cartesian body axes
Z/B	=	length of the relative chord
ξ	=	pitch-averaged energy loss coefficient
τ_{zx}	=	skin-stress component in the direction of x
τ_{zy}	=	skin-stress component in the direction of y

Subscripts

c	=	critical point
o	=	point on the separation line
1	=	inlet of the cascade
2	=	outlet of the cascade

I. Introduction

THE pattern of the limiting streamlines is always composed of several critical points for any given flow. Generally, the number, type, and distribution of the critical points are called the topological structure of the surface pattern. Through studying the local property of the critical points and their global character on the surface, we can discover much information on the flow. The application of topological analysis to fluid mechanics was started in the investigation on the behavior of limiting streamlines first adopted by Sears [1]. Legendre [2] went further into the postulate of continuous vector fields constructed by the limiting streamlines and studied the natures of singular points of finite number in the vector fields. So far, topological analysis has been widely and successfully used in the studies of external flows, such as those by Maskell [3], Lighthill [4], and Dellery [5], but rarely in the studies of internal flow, except by Delery and Meauze [6] and Gbadebo and Cumpsty [7]. Delery and Meauze made a detailed experimental analysis of the flow in a highly loaded compressor cascade and proposed a topological description. Gbadebo and Cumpsty described the three-dimensional character of corner separation in axial compressors by the principles of critical points.

Normally, secondary flow and secondary loss relate directly to the generation and evolution of various concentrated vortices, such as the passage vortex, horseshoe vortex, corner vortex, and trailing vortex in the blade passage. It is important to get a detailed knowledge of the vortices (with different separation types) in a typical cascade to control flow separation (different control methods may be adopted for different separation types), and to improve the performance. Several vortex patterns have been presented by many authors in the literature. For earlier work, we can refer to Hawthorne [8], Langston et al. [9], Goldstein and Spores [10], and Wang et al. [11] for a turbine cascade. In the last two decades, investigations on the vortex system in a compressor cascade have been performed by Cumpsty [12], Schulz et al. [13], and Kang [14].

It is well known that a compressor often operates at off-design conditions where the incidence changes significantly due to the variation of the pressure ratio, mass flow rate, and rotation speed. However, the effect of incidence on the flow structure, especially on the vortex structure, has not been investigated in detail thus far. The objective of this paper is to discuss the vortex structures at different incidences using the topological principles in a typical compressor cascade to supplement the knowledge of the vortex structure in a compressor cascade.

II. Numerical Procedure

The calculations were performed in a linear compressor cascade with a NACA65 profile using the CFD package Fine/Turbo of NUMECA. The code solves the full Reynolds-averaged Navier–Stokes equations on structured grids. A clear flow pattern is essential in this study. The quality of the numerical flow pattern is correlative with the number of the mesh nodes, value of y^+, and turbulence model. In this paper, the mesh consisted of $97 \times 49 \times 157$, in the radial (x), tangential (y), and streamwise (z) directions (see Fig. 1). And the value of y^+ was less than three. An explicit time marching, implicit residual smoothing four-step Runge–Kutta procedure and the turbulence model of k-epsilon (low Reynolds, see Yang and Shih

Received 19 April 2005; revision received 23 February 2006; accepted for publication 31 March 2006. Copyright © 2006 by the American Institute of Aeronautics and Astronautics, Inc. All rights reserved. Copies of this paper may be made for personal or internal use, on condition that the copier pay the $10.00 per-copy fee to the Copyright Clearance Center, Inc., 222 Rosewood Drive, Danvers, MA 01923; include the code $10.00 in correspondence with the CCC.

*Ph.D. Student, School of Energy Science and Engineering; hualiangzhang@163.com.

†Professor, School of Energy Science and Engineering; wang_stao@yahoo.com.

‡Professor, School of Energy Science and Engineering; wangzhongqi@hit.edu.cn.

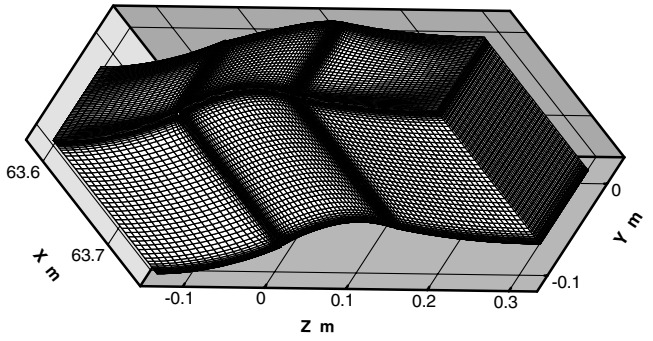

Fig. 1 Grid for the calculation.

[15]) were used in steady-state mode. Local time stepping and multigrid capability were applied to enhance convergence.

The inlet and exit boundary conditions were chosen to meet the real conditions of the cascade test, which was carried out in a low-speed wind tunnel at the Harbin Institute of Technology [16]. The total pressure and the total temperature at the inlet were 101830 Pa and 305 K, respectively; and the static pressure at the outlet was 99610 Pa.

III. Results and Discussion

A. CFD Validation

Figure 2 shows the radial distributions of the pitch-averaged energy loss coefficient at 40% of the chord length downstream of the blade trailing edge in the case of 0-deg incidence. The pitch-averaged energy loss coefficient is defined by

$$\bar{\xi} = \frac{(P_2/P_2^*)^{(k-1)/k} - (P_2/P_1^*)^{(k-1)/k}}{1 - (P_2/P_1^*)^{(k-1)/k}} \tag{1}$$

Figures 3 and 4 show the distribution of the limiting streamlines on the suction surface and endwall, respectively. It can be seen that the numerical results are consistent with the experimental results, which indicates that the numerical results of the current study have a certain level of accuracy.

B. Critical Principles of the Three-Dimensional Separation

There is clear evidence that separations in three-dimensional flows do not behave in the simple way that is associated with those in a two-dimensional case, where separation from the surface is identified at the point where the shear stress vanishes and by the inception of reversed flow. Three-dimensional separation can occur with no reverse flow and nonzero friction [17]. Let x, y, and z be the orthogonal coordinate system, with x and y lying on the body surface, y being the separation line, and z in the normal direction of the body surface. Zhang [18] proved the separation conditions to determine a three-dimensional separation line.

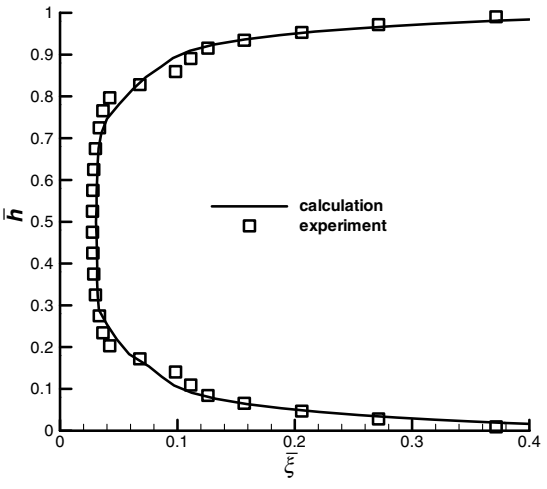

Fig. 2 Radial distribution of pitch-averaged energy loss coefficient.

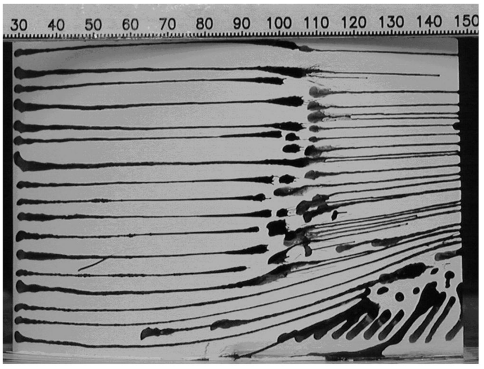

a) Experimental result

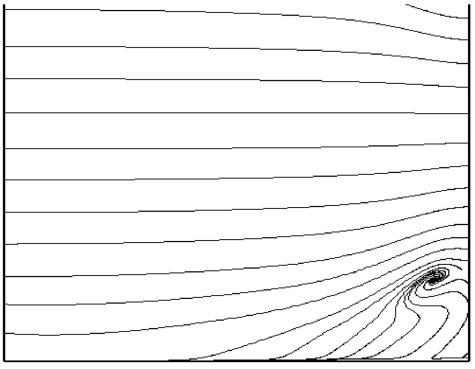

b) Numerical result

Fig. 3 Surface flow pattern on the suction surface.

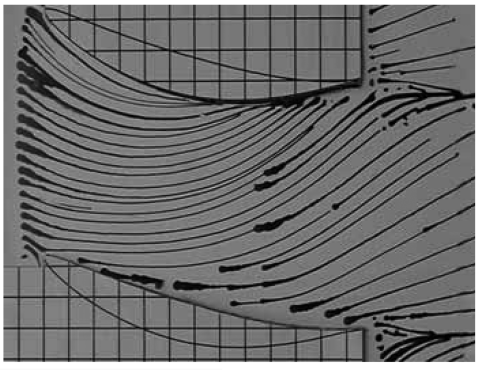

a) Experimental result

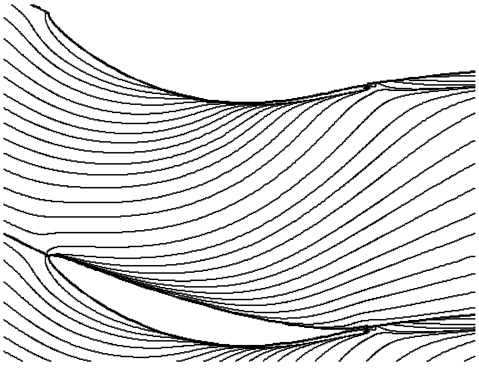

b) Numerical result

Fig. 4 Surface flow pattern on the endwall.

$$\left(\frac{\partial u}{\partial z}\right)_0 = 0, \qquad \left(\frac{\partial^2 u}{\partial x \partial z}\right)_0 < 0, \qquad \left(\frac{\partial^2 w}{\partial z^2}\right)_0 > 0 \tag{2}$$

where subscript "0" indicates the value taken from the point 0 on the separation line. So the shear-stress component of the x direction on the separation line satisfies the following rules:

$$(\tau_{zx})_0 = \left(\mu \frac{\partial u}{\partial z}\right)_0 = 0, \qquad \left(\frac{\partial \tau_{zx}}{\partial x}\right)_0 = \left(\frac{\mu \partial^2 u}{\partial x \partial z}\right)_0 < 0 \tag{3}$$

Suppose the point 0 is the origin of the coordinate; Taylor expressions of shear stress at the origin are obtained:

$$\tau_{zx} = (\tau_{zx})_0 + \left(\frac{\partial \tau_{zx}}{\partial x}\right)_0 x + \left(\frac{\partial \tau_{zx}}{\partial y}\right)_0 y + \ldots \tag{4}$$

$$\tau_{zy} = (\tau_{zy})_0 + \left(\frac{\partial \tau_{zy}}{\partial x}\right)_0 x + \left(\frac{\partial \tau_{zy}}{\partial y}\right)_0 y + \ldots \tag{5}$$

From Eq. (3), we can get the equation $(\partial^n \tau_{zx}/\partial y^n)_0 = 0$, where $n = 1, 2, 3, \ldots$. Consider the following expressions

$$f(x, y) = \left(\frac{\partial \tau_{zx}}{\partial x}\right)_0 + \frac{1}{2}\left(\frac{\partial^2 \tau_{zx}}{\partial x^2}\right)_0 x + \ldots \tag{6}$$

$$g(x, y) = \left(\frac{\partial \tau_{zy}}{\partial x}\right)_0 + \frac{1}{2}\left(\frac{\partial^2 \tau_{zy}}{\partial x^2}\right)_0 x + \ldots \tag{7}$$

According to the definition of the limiting streamline [2], we obtain the following equation:

$$\frac{h_2}{h_1}\frac{dy}{dx} = \lim_{h \to 0}\left(\frac{v}{u}\right) = \frac{\tau_{zy}}{\tau_{zx}} = \frac{x g(x, y) + (\tau_{zy})_0}{x f(x, y)} \tag{8}$$

It can be seen that the critical point of Eq. (8) is determined by the condition $(\tau_{zy})_0 = 0$ when the limiting streamline is a separation line (i.e., $x = 0$). Zhang and Deng [19] proved that the type of a critical point is determined by $(\partial \tau_{zy}/\partial y)_c$. If $(\partial \tau_{zy}/\partial y)_c > 0$, the critical point is a saddle point (a point through which two particular lines pass, each acting as barriers in the field of limiting streamlines or skin-friction lines, making one set of streamlines inaccessible to the adjacent set) [20]; if $(\partial \tau_{zy}/\partial y)_c < 0$, the critical point is a nodal point (a point around which an infinite number of limiting streamlines spiral, which, for example, can denote a vortex lifting off the surface) [20].

For the separation starting from a regular point (a point common to an infinite number of limiting streamlines) [20], which is the so-called open separation [21], because the direction of the shear-stress component τ_{zy} is always the same as that of the separation line (y being the separation line), the following conditions must be satisfied on the separation line:

$$(\tau_{zx})_0 = 0, \qquad (\tau_{zy})_0 > 0 \tag{9}$$

If a favorable pressure gradient is present along the separation line, which accelerates the flow, then the shear-stress component satisfies $(\partial \tau_{zy}/\partial y)_0 > 0$. So there will be no critical point $[(\tau_{zx})_0 = 0, (\tau_{zy})_0 = 0]$ occurring on the separation line. For the separation starting from a regular point, therefore, the critical points may occur only with an adverse pressure gradient. Furthermore, according to the principle for judging the critical point type, the first critical point on the separation line must be a nodal point or a saddle-nodal point (saddle point and nodal point are very close to each other), then the saddle point may occur next. That is because of $(\partial \tau_{zy}/\partial y)_0 < 0$ when the flow along the separation line is controlled under an adverse pressure gradient that decelerates the flow.

Based on the preceding discussions, we can infer that the variation of the critical points on the surface flow pattern, and the separation type in a compressor, is more sensitive than in a turbine because of the adverse pressure gradient. Note that the limiting streamlines are immediately adjacent to a solid surface so that they have the same directions as the shear-stress lines. The following discussions in this paper are based on the analysis of the limiting streamlines.

C. Topological Principles

1) For an annular or linear cascade with no clearance, stretch the casing and hub upstream and downstream far enough so that the flow is uniform, then bend them and connect the ends continuously (with no critical point at the joint). In topology, this cascade surface (blade surfaces and lower and upper endwalls) in a pitch is equivalent to a double cirque. It is known that the Euler characteristic of a double cirque is -2. According to the ideas of Poincaré [22], the total number of critical points on the limiting streamline pattern of the cascade surface must satisfy the following topological rule:

$$\sum N - \sum S = -2 \tag{10}$$

2) If the separation line starts from a critical point, this critical point must be a saddle point; if the separation line ends at a critical point, this critical point must be a nodal point [19].

3) If many critical points are distributed on the separation line, two saddle points or two nodal points cannot directly connect each other along the separation line, that is, the saddle point and the nodal point must appear alternatively [19].

D. Numerical Results and Discussion

The limiting streamlines on the suction surface and endwall at different incidences are shown in Fig. 5. Because the flow is attached on the pressure surface and there is no obvious radial secondary flow in all instances, the flow pattern on the pressure surface is not shown in this paper. It can be seen that the crossflow on the endwall increases with the increase of the incidence. The saddle point near the leading edge moves to the pressure side at positive incidence and

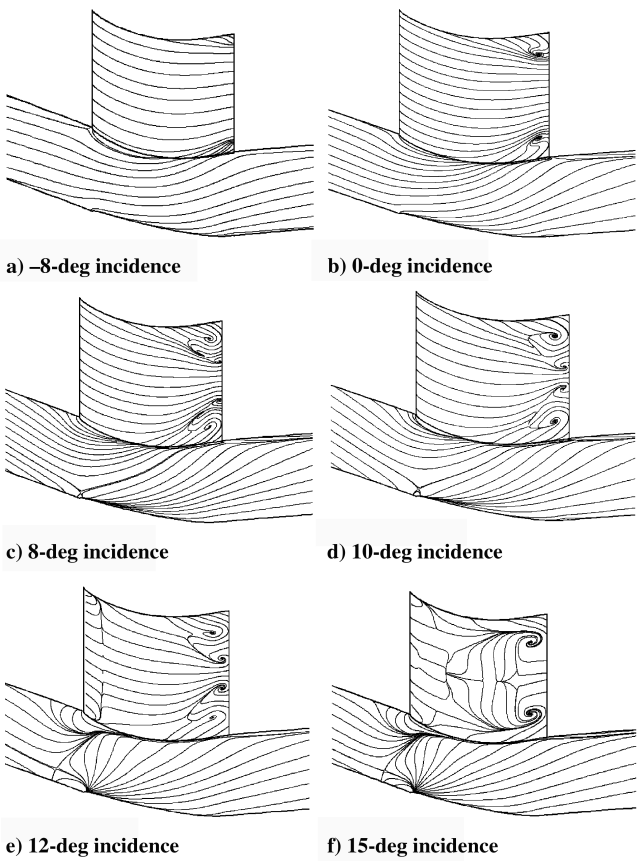

Fig. 5 Distributions of limiting streamlines on the suction surface and endwall.

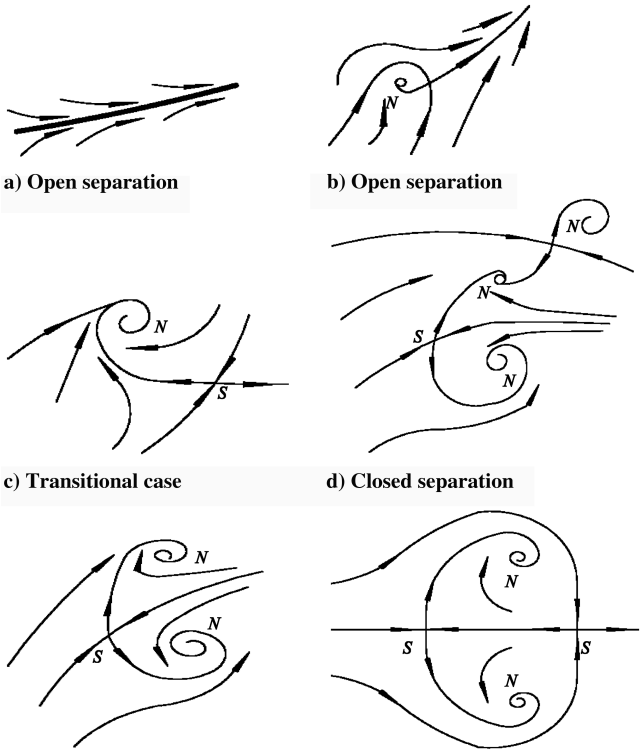

a) Open separation b) Open separation

c) Transitional case d) Closed separation

e) Closed separation f) Bubble formed

Fig. 6 Topology of the separation lines on the suction surface.

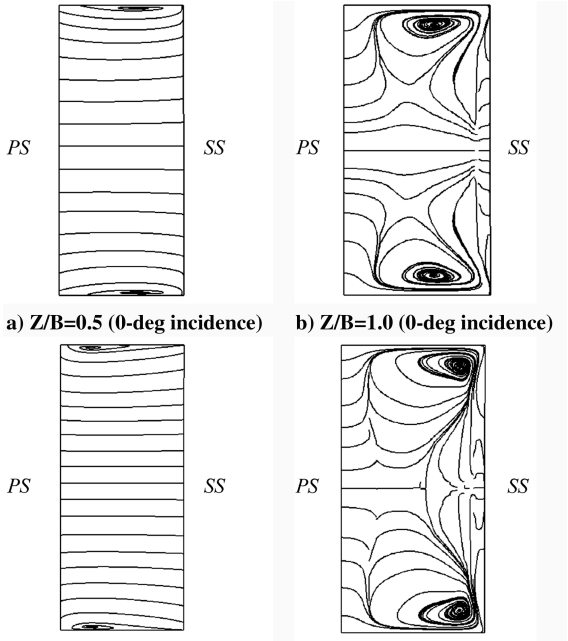

a) Z/B=0.5 (0-deg incidence) b) Z/B=1.0 (0-deg incidence)

c) Z/B=0.3 (10-deg incidence) d) Z/B=1.0 (10-deg incidence)

Fig. 7 Distributions of the cross velocity lines.

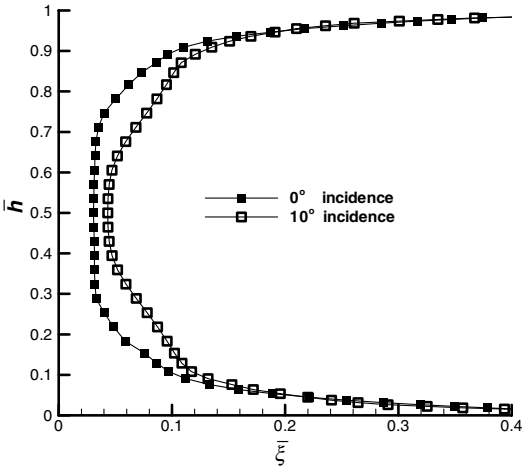

Fig. 8 Radial distribution of pitch-averaged energy loss coefficient.

near the suction side of the same blade at negative incidence. As the incidence increases, the separation line of the horseshoe vortex appears more and more clearly. The axial vorticity also shows the horseshoe vortex enhances, whereas its suction side leg eventually vanishes, because of the streamwise pressure gradient. The flow pattern on the suction surface varies remarkably. Figure 6a and 6b shows the development of the topological structure on the suction surface. We can see that, with the increase of the incidence, the separation type, originally open separation (Figs. 6a and 6b), then a transitional case (Fig. 6c), changes to closed separation (Figs. 6d and 6e) [21] and ultimately forms a bubble (Fig. 6f) in which the flow is very unsteady and the loss increases drastically. It is noticeable that there is a saddle-nodal point, as shown in Fig. 6b, which is a transitional structure between the critical point and the regular point. This variation of separation lines confirms the previous principle that regular points transit to critical points due to the adverse pressure gradient. The vortex structures under 0- and 10-deg incidences are compared in the following sections to discuss the effect of the incidence on the vortex structure in a compressor cascade.

Figure 7 shows the distribution of the streamlines at several traverse sections. The cores of the horseshoe vortex and the corner vortex cannot be seen from the figures, which proves that the intensity and scale of the horseshoe vortex are feeble. The development of the passage vortex can be observed clearly, and the original position of the seeable vortex core moves upstream as the incidence increases. In the case of 0-deg incidence, the core of the passage vortex can be observed at about 50% of the chord length downstream of the blade leading edge ($Z/B = 0.5$). When the incidence increases up to 10 deg, the passage vortex core occurs at about 30% of the chord length downstream of the blade leading edge ($Z/B = 0.3$). Note that the corner vortex still cannot be seen, which proves that it is tiny and not sensitive to the variation of the incidence. The pattern at the exit plane ($Z/B = 1.0$) shows the flow is more complex in the case of 10-deg incidence in comparison with that at 0-deg incidence, because of the change of the separation type.

Figure 8 shows the radial distribution of the pitch-averaged loss coefficient at 40% of the chord length downstream of the blade trailing edge. It can be seen that the flow loss increases distinctly with the increase of the incidence and the loss expands to the midspan. However, the variation of the pitch-averaged energy loss coefficient only occurs from 10 to 90% of the blade height, that is to say, the increase in loss mainly comes from the variation of the separation types on the suction surface. The energy loss coefficient near the endwall varies very little, which also proves that the corner vortex is not sensitive to incidence.

Although the variation of the incidence changes the behavior of the critical points, the relationship between the number of the saddle points and nodal points will be maintained according to the topological theory. Suppose that the flow is uniform far upstream and downstream, that is to say, all of the critical points are distributed on the surface of the cascade passage and there is no other critical point far away from the cascade. Figures 9 and 10 show the topology of the surface-limiting streamlines according to the numerical results by using the preceding topological principles. We can see that the total number of nodal points (including spiral points) is seven, and the total number of saddle points is nine, at different incidences. The bracket denotes the attachment nodal point N_m at the midspan, lying on the pressure surface. So the topological rule is satisfied (i.e., $\sum N - \sum S = 7 - 9 = -2$). It can be seen from the topology sketches that the crossflow from the pressure side to the suction side

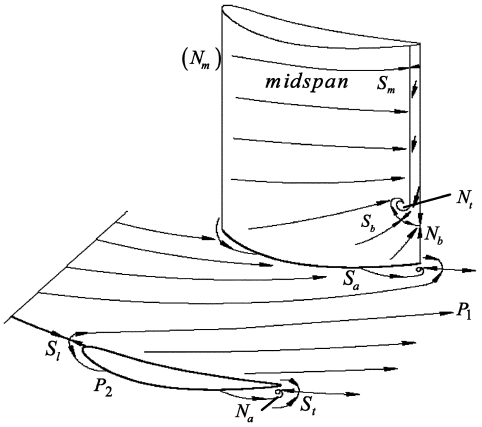

Fig. 9 Topology of surface flow pattern in the case of 0-deg incidence.

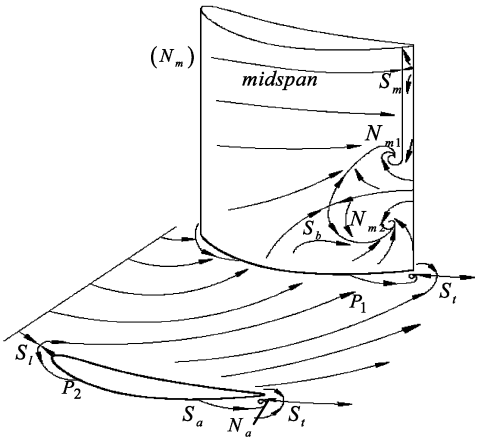

Fig. 10 Topology of the surface flow pattern in the case of 10-deg incidence.

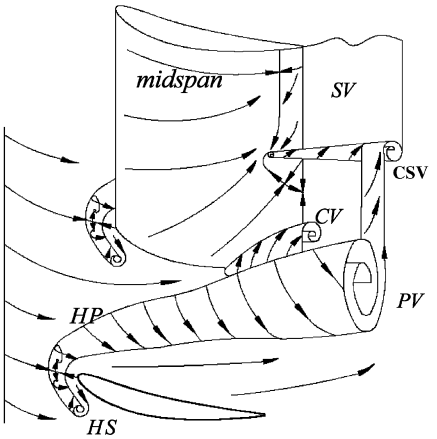

Fig. 11 Vortex structure in the case of 0-deg incidence.

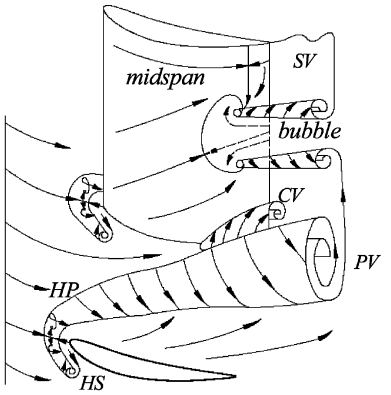

Fig. 12 Vortex structure in the case of 10-deg incidence.

strengthens visibly as the incidence increases. In the case of 0-deg incidence, the limiting streamline S_lP_1 flows outside without reaching the adjacent suction side. When the incidence increases up to 10_deg, however, the boundary layer on the endwall moves more strongly toward the suction side. The saddle point S_l moves to the midpassage and the limiting streamline S_lP_1 reaches the adjacent suction at about 70% of the chord length. In addition, we can see a separation line S_aN_a at the endwall near the suction surface, which is the separation line of the corner vortex. It is noticeable that the corner vortex does not come from the suction side leg of the horseshoe vortex. Its axial vorticity shows the rotation direction is opposite to the passage vortex. It can be inferred that the corner vortex is induced by the passage vortex and comes from the boundary layer on the endwall. On the suction surface, we can see that the pattern of the limiting streamlines alters distinctly with the increase of the incidence. In addition, there is a separation line (separation line S_mN_t at 0-deg incidence and separation line S_mN_{m1} at 10-deg incidence) near the trailing edge. This is the separation line of the tailing shedding vortex. It is not clear in the numerical flow pattern or in the oil visualization. Combining this information from the experiments or calculations with related topological principles, however, we can conclude this separation line.

The passage vortex is a classical open separation, which starts from a regular point so that the original position of the three-dimensional separation is difficult to be determined. We can only seek the approximate location through the pattern of cross velocity lines. The horseshoe vortex and the corner vortex start from a saddle point, and so they belong to closed separation. However, their separation surfaces after the saddle point are more similar to open separation and have the same formations as the passage vortex. The separation type changes notably on the suction surface. In the case of 0-deg incidence, the saddle point S_b and the nodal point N_b at the original position of the separation line are very close, which can be regarded as a transitional structure that the separation line starts from a saddle-nodal point. This separation line ends at the spiral point N_t and forms a so-called concentrated shedding vortex (CSV) [14]. The separation type is between open separation and closed separation. When the incidence increases to 10 deg, however, there are two separation lines labeled as S_bN_{m1} and S_bN_{m2} starting from a saddle point S_b. They end at spiral point N_{m1} and spiral point N_{m2}, respectively, and form two concentrated shedding vortices. This is the typical saddle point–spiral point separation that indicates that a distinct forbidden zone exists in the flow, and so it can be regarded as a closed separation. Based on the preceding analysis, a new model of the vortex system in a compressor cascade is proposed in Figs. 11 and 12.

IV. Conclusion

1) The variation of the critical points on the blade surface is complex because of the strong adverse pressure gradient in a compressor cascade; the separation on the suction surface is especially sensitive to incidence. The topology of the limiting streamline pattern on the suction surface varies with incidences, and the separation type translates into closed separation from open separation and ultimately forms a bubble that drastically increases the separation region and strength.

2) The passage vortex is a classical open separation in which the separation line starts from a regular point. The horseshoe vortex and the corner vortex belong to closed separation in which the separation line originates from a saddle point, and the vortex scale and the vortex intensity are tiny. Although the horseshoe vortex strengthens as the incidence increases, its suction side leg eventually vanishes due to the streamwise pressure gradient. The corner vortex is not sensitive to the variation of the incidence.

Acknowledgment

The authors would like to acknowledge the support of the National Natural Science Foundation of China, grant no. 50236020.

References

[1] Sears, W. R., "The Boundary Layer of Yawed Cylinders," *Journal of the Aero/Space Sciences*, Vol. 15, No. 1, 1948, pp. 49–52.

[2] Legendre, R., "Linges de Conrant d'un Ecoulement Coutinu," *La Recherche Aerospatiale: Bulletin Bimestriel de l'Office National d'Etudes et de Recherches Aerospatiales*, Vol. , No. 105, No. 1, 1965, pp. 3–9.

[3] Maskell, E. C., "Flow Separation in Three Dimensions," Royal Aircraft Establishment Rept. 2565, Farnborough Airfield, Nov. 1955.

[4] Lighthill, M. J., *Attachment and Separation in Three-Dimensional Flows, Laminar Boundary Layers*, edited by L. Rosenhead, Oxford Univ. Press, Oxford, 1963, pp. 72–82.

[5] Dellery, J., "Physique Des Ecoulements Tourbillonnaires," AGARD Rept. CP-494, 1990.

[6] Delery, J., and Meauze, G., "A Detailed Experimental Analysis of the Flow in a Highly Loaded Fixed Compressor Cascade: The Iso-Cascade Co-operative Programme on Code Validation," *Aerospace Science and Technology*, Vol. 7, 2003, pp. 1–9.

[7] Gbadebo, S. A., and Cumpsty, N. A., "Three-Dimensional Separations in Axial Compressors," American Society of Mechanical Engineers Paper GT2004-53617, 2004.

[8] Hawthone, W. R., "Rotational Flow Through Cascade," *Journal of Mechanics and Applied Mathematics*, Vol. 3, 1955, pp. 266–292.

[9] Langston, L. S., Nice, M. L., and Hooper, R. M., "Three-Dimensional Flow Within a Turbine Blade Passage," *Journal of Engineering for Power*, Vol. 99, No. 1, 1977, pp. 21–28.

[10] Goldstein, R. J., and Spores, R. A., "Turbulent Transport on the End Wall in the Region Between Adjacent Turbine Blades," *Journal of Heat Transfer*, Vol. 110, No. 101988, pp. 862–892.

[11] Wang, H. P., Steven, J. D., and Richard, J. G., "Flow Visualization in a Linear Turbine Cascade of High Performance Turbine Blades," American Society of Mechanical Engineers Paper 95-GT-7, 1995.

[12] Cumpsty, N. A., "*Compressor Aerodynamics*," Longman Scientific and Technical, Essex, England, U.K., 1989.

[13] Schulz, H. D., Gallus, H. E., and Lakshminarayana, B., "Three-Dimensional Separated Flow Field in the Endwall Region of an Annular Compressor Cascade in the Presence of Rotor-Stator Interaction: Part 1 —Quasi-Steady Flow Field and Comparison with Steady-Stator Data," *Journal of Turbomachinery*, Vol. 112, 1990, pp. 669–678.

[14] Kang, S., "Investigation on the Three-Dimensional Flow Within a Compressor Cascade With and Without Tip Clearance," Ph.D. Thesis, Dept. of Fluid Mechanics, Free Univ. of Brussels, Brussels, 1993.

[15] Yang, Z., and Shih, T. H., "New Time Scale Based on k-e Model for Near-Wall Turbulence," *AIAA Journal*, Vol. 31, No. 7, 1993, pp. 1191–1198.

[16] Song, Y. P., Zhao, G. J., Chen, F., and Wang, Z. Q., "Experimental Study of Sweep and Dihedral Effects on Compressor Cascade Performance," Air Flow Consulting Paper AFC-001, 2005.

[17] Chang, P. K., *Separation of Flow*, Interdisciplinary and Advanced Topics in Science and Engineering, Ser. 3, Pergamon, Oxford, 1970.

[18] Zhang, H. X., "Analytical Study of Three-Dimensional Separated Flows," *Progress in Natural Science*, Vol. 5, No. 2, 1995, pp. 238–240.

[19] Zhang, H. X., and Deng, X. G., "Analytic Studies for Three-Dimensional Steady Separated Flows and Vortex Motion," *Acta Aerodynamica Sinica*, Vol. 10, No. 1, 1992, pp. 8–19 (in Chinese).

[20] Dallmann, U., "Topological Structures of Three-Dimensional Flow Separation," DFVLR Rept. IB 221-82-A07, Proz–Wahn, Germany, 1983.

[21] Wang, K. C., "Separation Patterns of Boundary Layer Over an Inclined Body of Revolution," *AIAA Journal*, Vol. 10, No. 8, 1972, pp. 1044–1050.

[22] Poincaré, H., *Oeuvres de Henri Poincaré*, Tome 1, Gauthier–Villars, Paris, 1928.

F. Liu
Associate Editor